International Journal of Heat and Mass Transfer 52 (2009) 3118–3127

Contents lists available at ScienceDirect

International Journal of Heat and Mass Transfer

journal homepage: www.elsevier.com/locate/ijhmt

DNS study of pulsed film cooling for enhanced cooling effectiveness

Frank Muldoon [a], Sumanta Acharya [a,b,*]

[a] Center for Computation and Technology, Louisiana State University, Baton Rouge, LA 70803, USA
[b] Department of Mechanical Engineering, Louisiana State University, Baton Rouge, LA 70803, USA

ARTICLE INFO

Article history:
Received 29 January 2008
Received in revised form 14 January 2009
Accepted 14 January 2009
Available online 30 March 2009

Keywords:
Turbine airfoil cooling
Direct numerical simulations
Pulsed coolant jets
Cooling effectiveness

ABSTRACT

Direct Numerical Simulation (DNS) of a pulsed film-cooling jet is presented to examine if pulsations of the coolant jet can enhance film-cooling effectiveness. Calculations are performed for a cylindrical jet inclined at 30°. The jet pulsation is defined by the duty cycle (DC) and the Strouhal number (St), both of which are varied in this study. Baseline calculations are done for a steady blowing ratio of 1.5. Both frequency and duty cycle are observed to influence the cooling effectiveness. For a peak blowing ratio (M) of 1.5, pulsing with a St = 0.32 and DC = 0.5 is shown to reduce jet blow-off and improve centerline and spanwise-averaged effectiveness over the steady M = 1.5 case.

1. Introduction

The efficiency of turbine engines is directly proportional to the turbine inlet temperature. However, higher fluid temperatures can result in material limits being exceeded and can lead to blade failures. Therefore turbine components have to be cooled in order to prevent thermally induced material failure. A common means of cooling turbine blades is film cooling, in which the goal is to protect the blade surface from the hot crossflow by a film of cooler fluid injected through holes in the blade surface. These film-cooling holes must be designed in such a way that the coolant jet covers and remains near the blade surface and does not penetrate into the crossflow excessively. Mixing between the coolant and the crossflow is undesirable as this increases the temperature of the coolant. The film-cooling jets consume process air, and therefore a design goal is to maximize the cooling and minimize the mass flow through the jets. A desirable goal is to alter the geometrical or operational parameters of the coolant jets to improve cooling effectiveness. In this paper an approach for modulating the coolant jets is examined as a means for improving cooling effectiveness.

The aerodynamics in blade passages is an inherently unsteady process which has a significant impact on the film-cooling effectiveness [1]. In addition, with coolant injection, large-scale structures result from the interaction of the film-cooling jet with the crossflow. These large-scale structures and associated flow unsteadiness make it very difficult to predict the flow and heat transfer using the Reynolds Averaged Navier–Stokes (RANS) equations. For example the most commonly used turbulence model (the standard k–ε model) is well known to have difficulty in film-cooling applications. This model typically over predicts the distance the jet penetrates into the crossflow and under predicts the jet spreading rate [2–5].

There are very few studies in the literature concerning DNS or LES (Large Eddy Simulation) of film-cooling flows. An unsteady simulation of a circular jet in crossflow was performed by [6] on a $705 \times 161 \times 129$ grid using second-order central difference schemes. The Reynolds number was 1750 and the blowing ratio was 0.5. The delivery tube was not modeled in their work. They solved the incompressible Navier–Stokes equations but not the energy equation. Higher-order finite-difference schemes were used in an unsteady simulation by Muldoon and Acharya [7] to study a normally injected film-cooling jet which included the flow development in the delivery tube. They presented the unsteady interactions of the upstream crossflow and horseshoe vortex system with flow development in the delivery tube, and showed that this unsteady interaction resulted in a periodic pulsing of the jet. An LES of a film-cooling jet was done in a series of papers by Tyagi and Acharya [8–10] who investigated the influence of various parameters on the flow physics of square or rectangular coolant jets issuing normally into the crossflow, similar to the experimental setup of [11]. While the reported DNS/LES studies have shown improvements in predictive capabilities compared to Reynolds Averaged Navier–Stokes studies, due to the computational expense of DNS/LES, Reynolds Averaged Navier–Stokes (RANS) methods are the predominant industrial design tool for film-cooling flows.

The goal of this study is to computationally analyze the effect of external modulation (pulsing) on the coolant flow, and to examine if the film-cooling effectiveness is *enhanced or maintained the same*

* Corresponding author. Address: Department of Mechanical Engineering, Louisiana State University, Baton Rouge, LA 70803, USA.
E-mail address: acharya@me.LSU.edu (S. Acharya).

0017-9310/$ - see front matter © 2009 Elsevier Ltd. All rights reserved.
doi:10.1016/j.ijheatmasstransfer.2009.01.030

Nomenclature

η	film-cooling effectiveness = $(T_h - T_w)/(T_h - T_c)$
$\overline{\eta}$	spanwise spatially averaged film-cooling effectiveness
d	jet diameter
DC	duty cycle of pulsation
k	frequency in Hz
M	blowing ratio (U_{jet}/U_0)
Re	Reynolds number ($\rho U_0 D/\mu$)
St	Strouhal number (kd/U_0)
T_c	temperature of coolant
T_h	temperature of hot crossflow
T_w	temperature of wall
T	non-dimensional temperature = $(T - T_c)/(T_h - T_c)$
t	non-dimensional time = (td/U_0)
u, v, w	velocities in the streamwise, wall-normal and spanwise directions normalized by U_0
$u_{i,b}$	base jet-exit condition ($M = 1.5$)
U_{jet}	average velocity of jet
U_0	maximum crossflow velocity at the crossflow boundary
x, y, z	non-dimensional coordinates in streamwise, wall-normal and spanwise directions

with lower coolant mass flow utilization. As the problem is inherently unsteady (due to the external pulsing), the key to the successful prediction of such flows is the ability to resolve the dynamics of all important flow structures resulting from the interaction of the unsteady pulsed jet with the cross flow. As a result, time-averaged RANS solutions provide very little insight into the issues of interest in this work. A Direct Numerical Simulation (DNS) is therefore performed, and the results are used to examine the effects of pulsing on the flow.

A number of recent experimental studies have examined the potential of jet-modulation for film cooling [12–15]. Results from these studies have been mixed. For example, Coulthard et al. [14–15] report no enhancements in cooling effectiveness with pulsing while Ou and Rivir [12] have reported improvements in cooling with external pulsations. Because the earlier studies were experimental in nature, the available data needed to understand the mechanisms and provide a complete understanding was limited. In this study, we attempt to provide through DNS studies a more complete picture of how pulsations influence the flow and temperature fields, and how the cooling effectiveness is influenced.

2. Governing equations and numerical solution

The governing equations of interest in this work are the non-conservative unsteady three-dimensional Navier–Stokes equations (Eqs. (1) and (2)) in their incompressible form. In addition, an equation describing the evolution of a passive scalar, considered here to be the temperature (Eq. (3)), is solved. These equations are solved without the use of a model for turbulence. Eqs. (1)–(3) are solved in non-dimensional form (velocities normalized by U_0 and lengths normalized by d), in which the properties of the fluid and the temperature are described by the Reynolds number (Re) and the Prandtl number (Pr).

$$\frac{\partial u_i}{\partial t} + u_j \frac{\partial u_i}{\partial x_j} = -\frac{\partial p}{\partial x_i} + \frac{1}{\mathrm{Re}} \frac{\partial^2 u_i}{\partial x_j} \tag{1}$$

$$\frac{\partial u_i}{\partial x_i} = 0 \tag{2}$$

$$\frac{\partial T}{\partial t} + u_j \frac{\partial T}{\partial x_j} = \frac{1}{\mathrm{Re.Pr}} \frac{\partial^2 T}{\partial x_j} \tag{3}$$

The solution to the above system of equations is achieved using Direct Numerical Simulations (DNS) that embody higher-order finite-difference discretization (with low truncation errors), and a highly resolved mesh that captures all the necessary length scales in the inertial subrange. A fourth-order central difference scheme with a monotonic limiter is used for the convective terms. Fourth-order interpolation for the velocity in the convective terms, e.g. for v in $v\frac{\partial u}{\partial y}$, etc. is used. A fourth-order central difference scheme is used for the diffusive terms. A third-order accurate explicit time integration scheme is used to integrate the convective and diffusive terms in time. The pressure gradient and the continuity equation are represented by second-order centered schemes. The equation for temperature is represented using the same order and type of schemes used for the momentum equations. To solve the resulting system of discretized equations, a colored Symmetrically Coupled Gauss–Seidel (SCGS) scheme is used. Three subiterations per physical time step are used in the colored SCGS method. Solutions are obtained from an in-house computer code using the Message Passing Interface (MPI) and Fortran 95 for parallel computer architectures.

The DNS nature of the code has been demonstrated by solving a number of benchmark problems including turbulent fully developed channel flow and turbulent separated flow past a backstep. These results are reported in Muldoon [16] and Muldoon and Acharya [17], and demonstrate that the predictions are in excellent agreement with measurements and published results for these two benchmark problems, and that the inertial subrange is effectively captured (the energy spectra captures the $-5/3$ inertial subrange region). Further details of the finite-difference schemes, the DNS computer code used in this work and validation studies are given in [16,17].

3. Problem definition

A schematic of the flow domain along with boundary conditions and dimensions is given in Fig. 1. A cylindrical inclined jet at 35° inclination to the surface is considered. The calculation domain for the pulsed jet simulations are shown in Fig. 1, with prescribed jet-exit conditions. As described later, the baseline jet-exit conditions are obtained from a separate DNS calculation that included the coolant delivery tube. The dimensions of the computational domain are $L_{up} = 3.6$ d, $L_{down} = 14$ d, $L_{freestream} = 4.5$ d, $L_z = 3$ d. The grid spacing is non-uniform in the x, y and z directions to increase resolution near the jet exit and the wall. The ratio of the maximum to the minimum grid spacing is 2.13, 3.83 and 1.34 in the x, y and z directions, respectively.

Due to the assumption of incompressibility, the flow field considered is essentially subsonic, and density variations are small. We have further assumed that the temperature differences between the coolant jet and the crossflow are not large, and hence the density ratio of the coolant jet to that of the crossflow is nearly unity. The density ratio is therefore not accounted for in the definition of the blowing ratio M (defined as the ratio U_{jet}/U_0). For flows where the density ratio is substantially greater than 1, the jet to crossflow momentum ratio will be higher for the same velocity ratio, and may play a role in the flow dynamics near the jet-exit region. This aspect is not considered here.

Periodic boundaries are used in the z direction. A symmetry boundary condition is applied at $y = L_{freestream}$. A convective outflow boundary condition is applied for all three velocities at $x = L_{down}$. At the jet exit, time averaged results obtained from an-

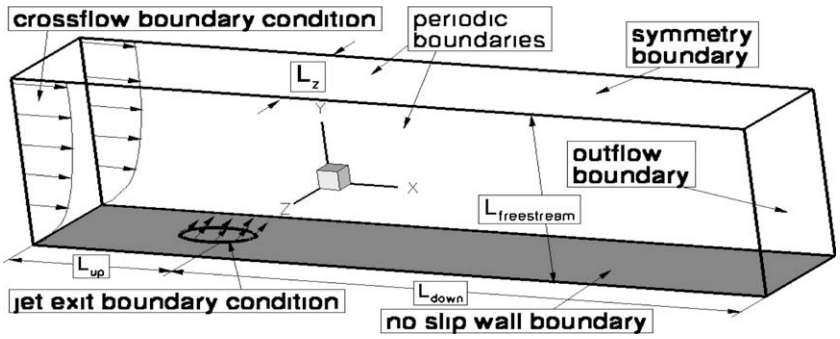

Fig. 1. 3D schematic of inclined jet in crossflow with prescribed jet-exit velocity.

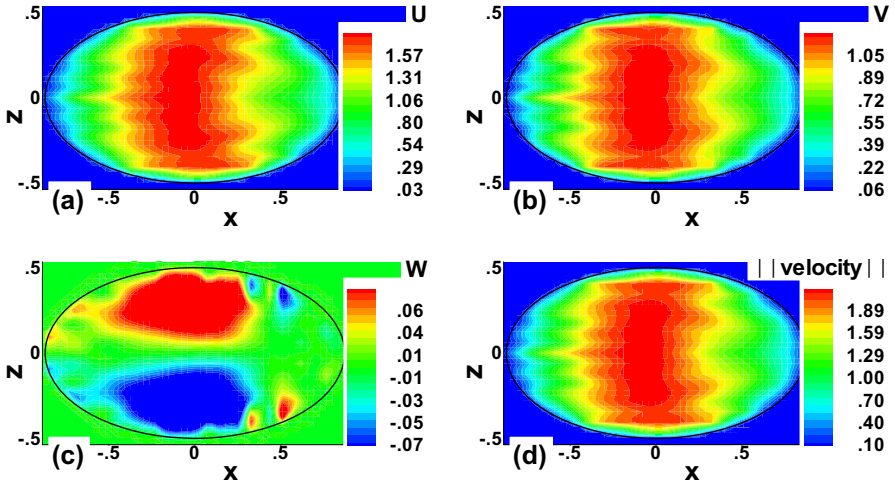

Fig. 2. Temporally averaged jet-exit boundary condition obtained from simulation which included delivery tube, non-dimensionalized by U_{jet} (no pulsing).

other simulation which included the delivery tube are used as a boundary condition for the velocity. The average blowing ratio M is 1.5, where the U_{jet} is the mean velocity parallel to the coolant hole orientation (35°). For the simulation that includes the delivery tube, U_{jet} is simply the average velocity inside the delivery tube and the length to diameter of the coolant delivery tube is taken to be 3.5 which is typical for many film-cooling configurations. Fig. 2 shows the contours of the three velocity components along with the velocity magnitude at the jet exit. Pulsing of the jet is realized by temporally modulating this boundary condition. For the unpulsed cases at lower blowing ratios than 1.5, to keep the comparison focused on the exit jet–crossflow interaction alone, the jet-exit velocities are simply scaled relative to the 1.5 blowing ratio case, and are obtained by reducing all three components of the velocity boundary condition at the jet exit as found by the $M = 1.5$ simulation with a delivery tube, and such that the correct blowing ratio is obtained.

To rationalize the above choice of the jet-exit boundary condition, it should be noted that the goal of the paper is to examine how coolant jet pulsations effects the mixing and heat transfer performance. The simplest thing to do would have been to use a flat jet-exit profile or an assumed fully developed profile at the jet exit, and indeed such assumptions have been done in the literature (see review of film-cooling computations by Acharya et al. [18]). The other extreme is to include the delivery tube and the plenum in all the calculations, but this would have required the mesh size to have increased significantly if the same resolution was maintained in the tube and plenum region as above the jet or would have required this resolution to be lower if the total number of grid points were kept the same. Given the grid independence study we performed, the latter option (lowering the mesh resolution) was not viable. Therefore the compromise reached was to maintain the needed resolution above the jet exit, but specify a realistic boundary condition based on time-averaged results. Therefore, for the blowing ratio of 1.5, a complete DNS calculation was done including the coolant delivery tube and the plenum, time-averaged results were generated at the jet exit. This time-averaged jet-exit profile was then used as a boundary condition with appropriate addition of modulation (for pulsed cases) and scaling for other blowing ratios as explained earlier.

At the crossflow inlet boundary at $x = L_{up}$, the v and w components of velocity are set to zero while a 1/7th-law velocity profile is used for the u velocity (Eq. (4)). The freestream turbulence intensity is considered to be very small and no velocity perturbations

$$u = U_o(y/\delta)^{1/7} \tag{4}$$

are introduced at the inlet to the computational domain. This boundary condition is used to simulate low freestream turbulence, and also for computational expediency, as imposing inlet turbulence involves additional computational effort to achieve time accurate boundary conditions for DNS. This would involve running a separate simulation and storing a large amount of data to provide a turbulent boundary layer, or greatly extending the domain upstream to allow tripping the boundary layer and permitting it to develop. The authors believe that it is better to utilize the limited computational resources in resolving the region where the jet and crossflow interact.

The Reynolds number based on U_0 and jet diameter is 8000, the Prandtl number is one (representing a gaseous medium such as air). A constant density independent of temperature is used for both the jet and crossflow since the temperature differences between the two streams are assumed to be small. A non-dimen-

sional value of one is specified for the boundary conditions for the temperature at the crossflow inlet boundary and freestream. A convective outflow boundary condition is applied at the outflow, while a first order no-flux (adiabatic) boundary condition is applied at the wall. Within the jet exit a Dirichlet boundary condition of zero for the non-dimensional temperature is applied. The time step used to integrate Eqs. (1)–(3) results in maximum CFL numbers of ~0.12 in the x and y directions and ~0.06 in the z direction.

4. Pulsing scheme

The pulsing is controlled by two variables, the duty cycle (DC) and Strouhal number (St). The duty cycle is defined as the ratio of the time that the jet is on over the total time. When the jet is off it is completely shut off. The Strouhal number is defined as $\frac{kd}{U_0}$, where k is the frequency in Hz, d is the coolant hole diameter and U_0 is the crossflow velocity. The velocity at the jet exit is varied according to Eq. (5), where $u_{i,b}$ is the ith component of velocity at the jet-exit plane obtained from the simulation including the delivery tube (as shown in Fig. 2) and a is a step function, being either 0 or 1.

$$u_{ib} = u_i^b a \tag{5}$$

The integral of a over time as time goes to infinity equals the duty cycle. Therefore, for pulsed cases the average blowing ratio is DC × 1.5 while the peak blowing ratio (during the "on" part of the blowing cycle) is always 1.5 for all cases studied.

Seven different cases are reported in this work. These cases were selected from a preliminary study that involved forcing frequencies over a broader range: St = 0.004–0.32. The cases examined in detail are:

Unpulsed (St = 0): (M = 1.5), (M = 0.75), (M = 0.375),

Pulsed: (DC = 0.5, St = 0.08, M = 0.75), (DC = 0.5, St = 0.32, M = 0.75), (DC = 0.25, St = 0.08, M = 0.375), (DC = 0.25, St = 0.32, M = 0.375).

Note that for the unpulsed cases (St = 0), three steady blowing ratios (1.5, 0.75 and 0.375) are considered. The blowing ratio indicated in the figures for the pulsed cases is an average blowing ratio with the peak blowing ratio for all the pulsed cases at 1.5. A smaller DC implies a lower average blowing ratio and a lower integrated coolant flow rate. To provide a baseline for comparison, we will use the unpulsed (St = 0) case with M = 1.5, since all the pulsed cases have the same peak blowing ratio of 1.5. If the film-cooling effectiveness for the pulsed cases achieve or exceed the baseline unpulsed case (M = 1.5), it implies that the same or greater cooling effectiveness is achieved with lower coolant flow rates. For comparison purposes, we will also present simulation results for unpulsed cases with lower coolant mass flow rates (lower blowing ratios of M = 0.75 and 0.375). However, it should be noted that achieving the lower blowing ratios in practice may be impractical due to concerns regarding ingestion into the coolant holes.

It should be noted that duty cycle and frequency are independent parameters. Keeping the duty cycle the same and changing the frequency does not alter the coolant mass flow rate. However, changing the duty cycle does alter the coolant mass flow rate; for example, a lower duty cycle (smaller percentage of time when the valve is open) implies a lower coolant flow rate.

5. Metrics

The effectiveness of the film-cooling jets is measured by the film-cooling effectiveness η, which is defined by Eq. (6), where T_h is the temperature of the hot incoming fluid, T_w is the temperature of the wall and T_c is the temperature of the coolant.

$$\eta = \frac{(T_h - T_w)}{(T_h - T_c)} \tag{6}$$

The spanwise average film-cooling effectiveness $\overline{\eta}$ is obtained by integrating the local cooling effectiveness across the hole-pitch (±1.5 d), defined by Eq. (7), and is used throughout this work to compare results for the various cases studied.

$$\overline{\eta}(x) = \frac{1}{3d}\int_{-1.5d}^{1.5d} \eta(x,z)dz \tag{7}$$

6. Grid independence

A key issue in numerical solutions of Eqs. (1)–(3) is the elimination of the effect of the grid spacing on the solution. In this work, this independence of results from the grid is verified by using a sequence of grids. These grids are related to each other in that each coarser grid is obtained from its next finest by removing every other grid point in each dimension. Four grids, with dimensions of 185 × 49 × 40, 369 × 97 × 80, 737 × 193 × 160 and 1473 × 385 × 320 are used. The time step is reduced by half when moving from one grid to the next finest grid. An important metric in this work is the film-cooling effectiveness. Grid independent results for the film-cooling effectiveness can be seen in Fig. 3 for the 737 × 193 × 160 and 1473 × 385 × 320 grids. The results shown in this work are obtained on the 737 × 193 × 160 grid (nearly 23 million grid points). As further validation, DNS results have been compared with experimental data and shown to agree well with measurements [16,18].

If statistical data is desired, then the time period and frequency with which the statistical data is collected must be addressed. In this work, statistics are collected at each discrete time step. No noticeable difference was found in the film-cooling effectiveness when the time period over which statistics are collected is doubled. In this work all statistics are obtained by averaging in time over 216 non-dimensional units of flow-through time. Thus, both from the perspectives of grid resolution and time period for averaging, these calculations generally exceed those available in the reported literature.

7. Results and discussions

Jets in crossflow contain a number of distinct flow structures as described by Coulthard et al. [14,15]. For accurate simulation of mixing and transport, it is important that the energy-carrying structures be correctly simulated, and therefore DNS or Large Eddy

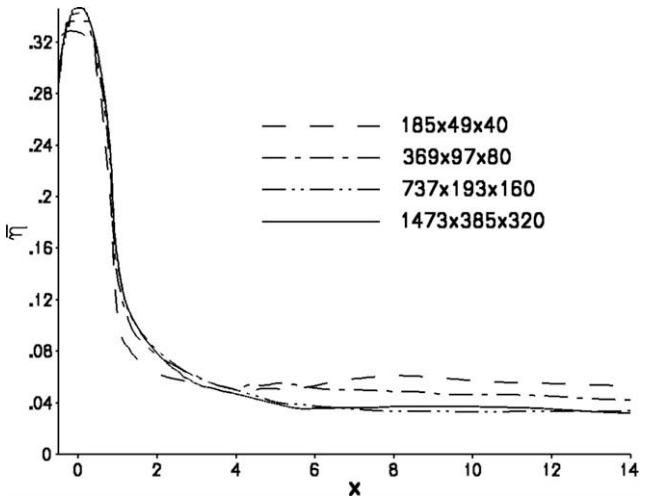

Fig. 3. Spanwise-averaged film-cooling effectiveness on different grids, St = 0.04, DC = 0.25.

Simulation (LES) techniques are needed for this purpose. While the focus of this paper is on the scalar transport it is important to recognize the role of these structures since they play an important role on the mixing. These structures for the film-cooling configuration include: the Counter Rotating Vortex Pair (CVP) represented by kidney shaped vortices, a horseshoe vortex, shear-layer vortices and upright wake vortices [19]. As the jet is deflected by the crossflow it splits into the CVP. While it is difficult to distinguish the CVP in an instantaneous image of the flow field, it can be clearly seen if the time-averaged flow field is examined. The CVP entrains fluid from the crossflow into the jet, promoting mixing of the jet with the crossflow. As a result of vortex induction, the CVP causes the jet to lift away from the surface, which is undesirable for film cooling. The horseshoe vortex forms close to the wall upstream of the jet, wraps around the jet, and reorients itself in the streamwise direction. Its role is to entrain coolant fluid from the jet and to cool the blade surface along its trajectory. Shear-layer vortices form at the boundary between the jet and the crossflow. These vortices begin small but grow into large-scale structures by 3–4 d downstream of the jet center. Wake vortices are not seen in the flows in this work, likely as a result of the low blowing ratio and small jet inclination angle (which results in a jet close to the blade surface). While these flow structures influence the mixing and surface temperatures, in the results presented below, we will focus primarily on the cooling effectiveness and the scalar temperature distributions. The signature of these flow structures (and particularly the leading edge shear-layer vortices and the wake generated vorticity) is however evident in examining the contours of the scalar transport presented here.

7.1. Unpulsed cases

Fig. 4 shows instantaneous images of the temperature field showing the downstream development of large-scale shear-layer vortical structures and the lack of reattachment of the jet at $M = 1.5$. In particular, there is no starting vortex which will be shown later in the pulsed cases to play a key role in altering the behavior of the jet and causing the jet to reattach to the surface. However, the evolution of the leading edge shear-layer vorticity can be seen in Fig. 4, and appear to manifest themselves clearly around $x = 3$–4. The entrainment of the crossflow (hot) below the coolant jet is clearly evident. A distinct separation is seen till about $x = 4$, but even beyond this, the penetration of the crossflow below the coolant jet is evident and effective cooling of the surface is not observed.

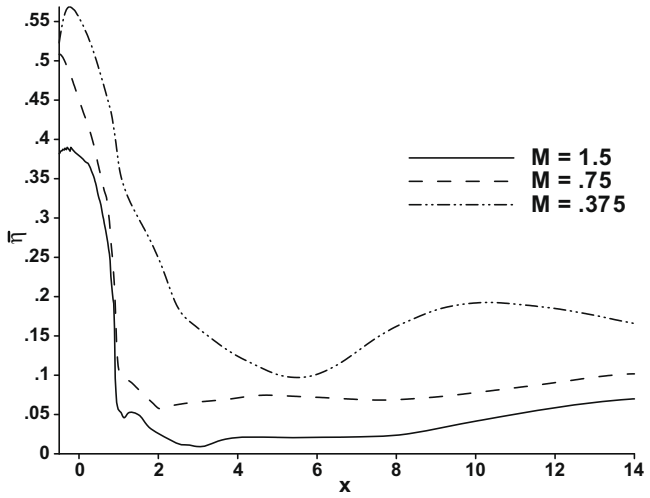

Fig. 5. Spanwise-averaged film-cooling effectiveness, unpulsed cases.

Fig. 5 shows the spanwise-averaged film-cooling effectiveness plotted as a function of the streamwise distance. Note that the spanwise averaging is done over the entire 3 d spanwise dimension, and as can be seen later in the surface contour plots (Fig. 7) the lateral spreading of the coolant is limited, and therefore the spanwise-averaged values are expected to be low. At $M = 1.5$, as shown in Fig. 4, the jet blows-off in the near-field, and spanwise-averaged cooling effectiveness values are quite low. An increase in the film-cooling effectiveness is obtained as the blowing ratio is reduced. Reducing the blowing ratio causes the jet to adhere closer to the surface. This behavior of the jet as the blowing ratio is reduced can be clearly seen in the time-averaged temperature contours of Fig. 6 where the penetration of the jet into the freestream is greatly reduced with decreasing blowing ratio. Reducing the blowing ratio also greatly reduces the recirculation region behind the jet (compare Fig. 6a and c). Fig. 7 shows the contours of the wall-temperatures and demonstrates that at the higher blowing ratio of 1.5 the coolant blows-off the surface and the surface is mostly at the crossflow temperature. As the blowing ratio is reduced to 0.75, the signature of the coolant reattachment is evident around $x = 4$, while at $M = 0.375$ the jet is fully attached. Fig. 7 also shows that the ingestion of coolant by the horseshoe vortex is greatly increased as the blowing ratio is reduced. This ingestion

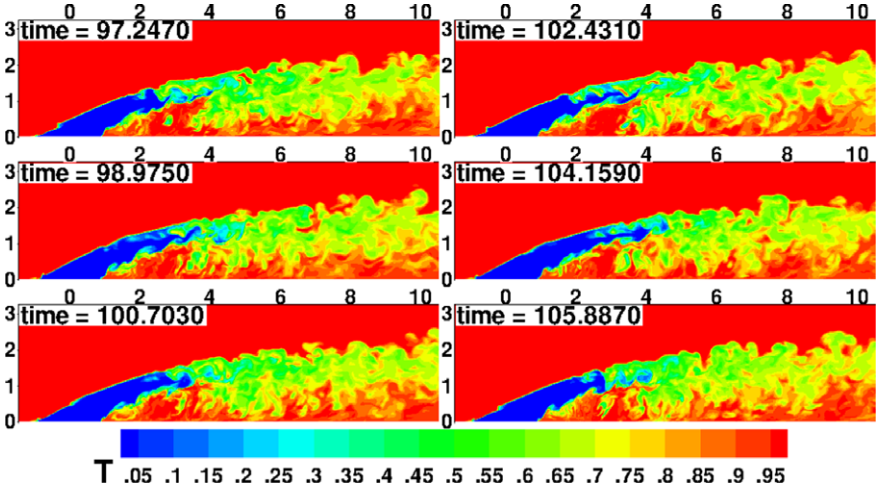

Fig. 4. Temperature contours at different time instances, unpulsed case, $M = 1.5$, $z = 0$, horizontal axis is x, vertical axis is y.

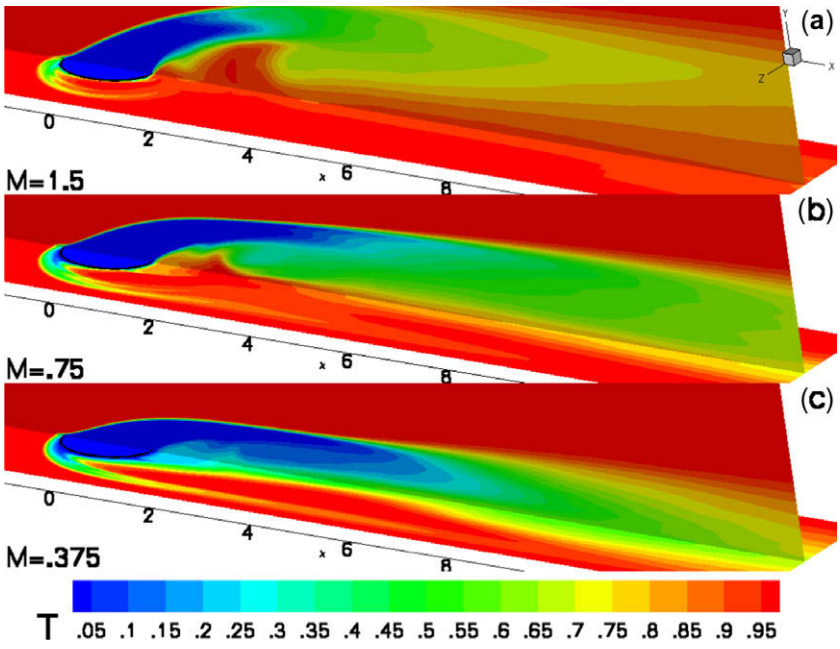

Fig. 6. Contours of mean temperature, unpulsed cases.

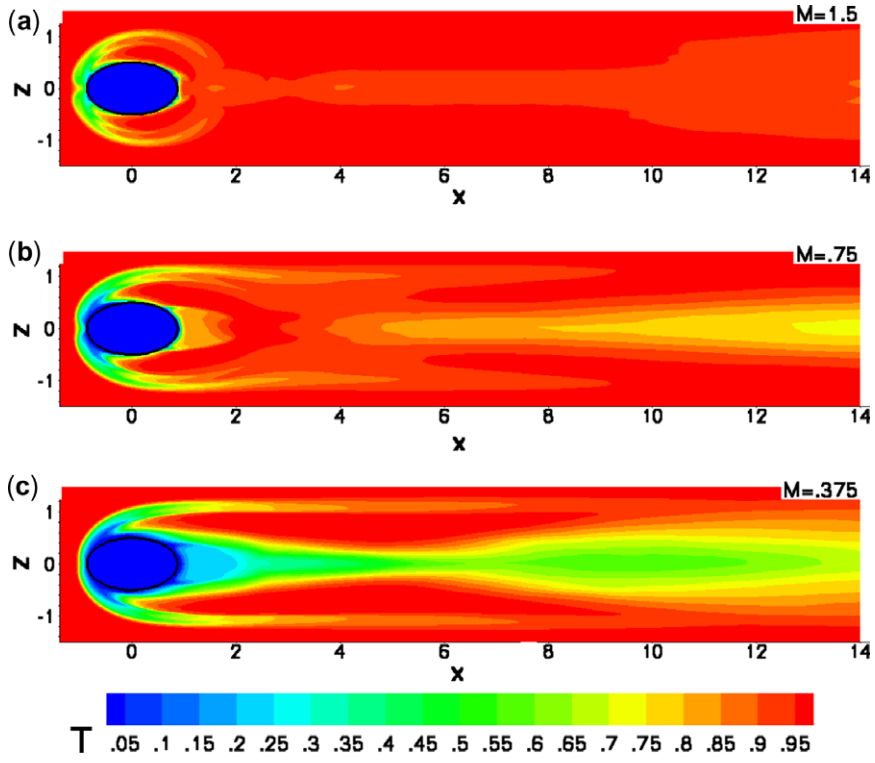

Fig. 7. Contours of mean temperature on the wall, unpulsed cases, horizontal axis is *x*, vertical axis is *z*.

is beneficial since the vortex remains close to the blade surface and therefore protects it. This figure also clearly shows the improved cooling on the blade surface as the blowing ratio is reduced. However, it is important to remember that to achieve an average blowing ratio of 0.375, the average pressure ratio across the coolant hole must be relatively low, leading to local pressure ratios at the jet exit that may permit the hot crossflow to be ingested into the hole. This is clearly undesirable, and therefore, in practice, coolant jet blowing ratios in the 1–2 range are commonly used.

7.2. Pulsed cases

In making a comparison of the pulsed and unpulsed cases, a key issue is the baseline case against which the comparison should be made. An obvious choice is to use the 1.5 steady blowing ratio case as the basis for comparison since the peak blowing ratio for all pulsed cases is 1.5. It will be seen that with this choice as the baseline, pulsing generally produces an improvement in film-cooling effectiveness (Fig. 8). It should be noted that pulsing reduces the

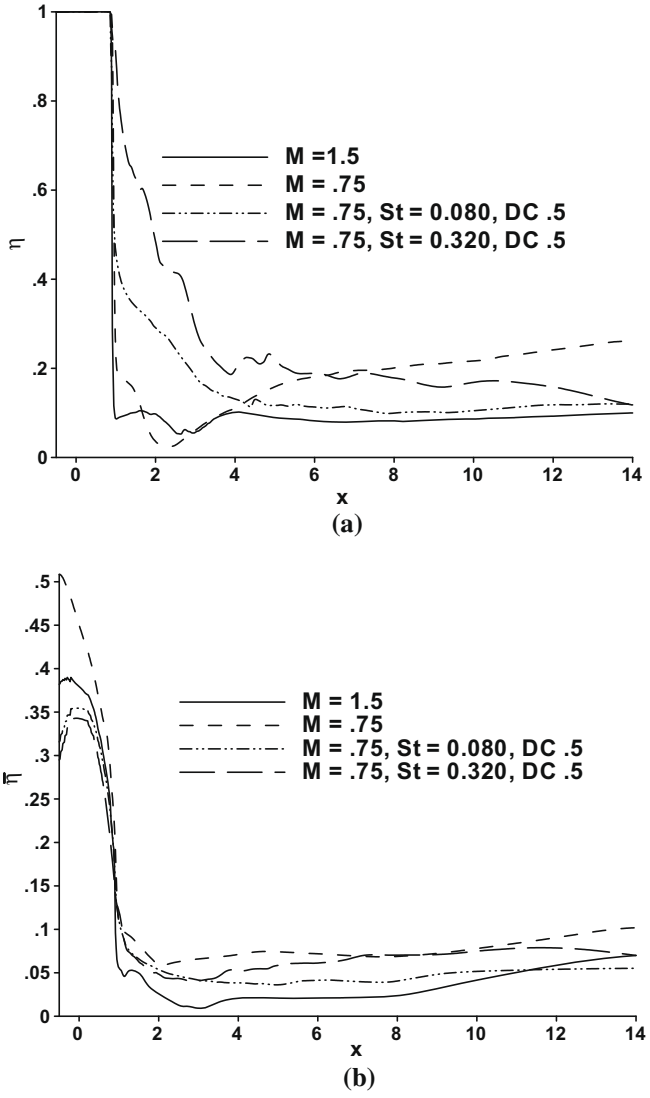

Fig. 8. (a) Centerline and (b) spanwise-averaged film-cooling effectiveness, unpulsed and DC = 0.5.

total coolant mass flow rate since the jet is off for a certain duration of the cycle. Therefore, the effective blowing ratio is smaller than 1.5 with pulsing (less coolant is used), and another case for comparison is to use steady jet with the lower effective blowing ratio. However, as mentioned above steady values of low blowing ratios are difficult to sustain due to ingestion issues. While it may be argued that during the "low" or "off" part of the pulsing cycle, the potential of ingestion into the coolant hole also exists, it should be noted that the low part of the cycle persists for only a short duration (depending on the duty cycle), and the dynamics leading to ingestion take time to establish themselves. This time needed for the ingestion to establish itself may be longer than the time for which the "low" part of the cycle is on. Further, the low part of the pulsing cycle can be adjusted to be above the threshold ingestion levels. While more studies are needed to establish the above arguments, it should be noted that the main purpose of the paper was to demonstrate that for a certain blowing ratio (say 1.5), adding pulsations improves the cooling effectiveness, and this has the added benefit that it decreases the coolant needed.

Fig. 8 shows the effect of pulsing at an average blowing ratio of 0.75 (peak blowing ratio of 1.5) and two pulsing frequencies along with the baseline case of an unpulsed jet at blowing ratios of 1.5, and the unpulsed case with the same average blowing ratio as the pulsed cases (0.75). Fig. 8(a) shows the centerline cooling effectiveness while Fig. 8(b) shows the spanwise-averaged values. Compared to a peak blowing ratio of 1.5, both cases of pulsing improve the cooling effectiveness. In particular, the centerline values immediately downstream of the hole see significant increases in cooling effectiveness (factor of 3–5). Pulsing at a Strouhal number of 0.32 is seen to be more beneficial than 0.08. However when the pulsed cases are compared with a steady blowing ratio of 0.75, pulsing produces improvements in the centerline film-cooling effectiveness in the near-vicinity of the coolant hole (upstream of x of about 4). The spanwise-averaged cooling effectiveness at a Strouhal number of 0.32 has a similar film-cooling effectiveness as the case with the 0.75 blowing ratio with no pulsing except in the very-near-hole region where the unpulsed case shows higher effectiveness due to the additional cooling induced by the horseshoe vortices. However, if the $M = 1.5$ unpulsed case is used as the baseline, the pulsed cases do represent an improvement over the baseline case. This improvement is due, in part, to changes in the vortex dynamics (explained later), and the accompanying reduction in effective blowing ratio associated with pulsing. Note that this improvement in cooling effectiveness is also accompanied by a 50% reduction of the coolant usage, and therefore compared to the unpulsed baseline of $M = 1.5$, there is a dual benefit of pulsing at St = 0.32, DC = 0.5, that of reduction in coolant usage and increase in cooling effectiveness.

Fig. 9 shows the spanwise distribution of film-cooling effectiveness at four locations downstream of the coolant injection ($x = 2$, 6, 10, 14). The higher peak spanwise distributions for the two pulsed cases relative to the baseline unpulsed case ($M = 1.5$) are clearly evident over most of the spanwise extent of the coolant jet. In the near-field ($x = 2$), the peak effectiveness is nearly 3 times higher at St = 0.08 and over 4.5 times higher at St = 0.32. As far downstream as $x = 10$, pulsations show clear benefits for St = 0.32. Interestingly, for the unpulsed $M = 0.75$ case, the near-field ($x = 2$) shows a different pattern with two peaks offset from the centerline. These dual-peaks are a reflection of the stronger role of the horseshoe vortices at the lower blowing ratio. The horseshoe vortices entrain the coolant air along the leading edge of the coolant jet, and stays close to the wall as it wraps around the coolant jet. Evidence of this behavior is seen in Fig. 7, where the trace of the horseshoe vortex can be clearly seen at blowing ratios of 0.75 and 0.375.

One adverse impact of pulsation appears to be a slight spanwise contraction of the coolant jet. This is seen in Fig. 9 where for $Z > 1$ or $Z < -1$ the unpulsed case has slightly elevated cooling effectiveness. However, at these locations, sufficiently removed from the centerline, the cooling effectiveness is generally low (except in the near-field where the presence of the horseshoe provides increasing cooling effectiveness), and the slight contraction of the coolant jet with pulsing has a negligible effect on the spanwise-averaged effectiveness.

Fig. 10 shows the temperature contours along the mid-plane ($Z = 0$) and along the wall for the two pulsed cases. The corresponding unpulsed case contours are shown in Fig. 6. Pulsing at St = 0.32 results in a reduction of the separation of the coolant jet (compare Fig. 10b with Fig. 6a for $M = 1.5$ or Fig. 6b for $M = 0.75$). Therefore, the poor protection of the blade in the recirculation region immediately behind the jet is greatly improved with pulsing. However, pulsing completely destroys the horseshoe vortex. This destruction of the beneficial horseshoe vortex is the reason why pulsing limits the improvement in the film-cooling effectiveness.

Turning attention to a lower duty cycle of 0.25, Fig. 11 shows that for a duty cycle of 0.25, pulsing at a Strouhal number of 0.08 results in comparable or slightly higher film-cooling effectiveness than at a Strouhal number of 0.32. Compared to the baseline case of the unpulsed $M = 1.5$ coolant jet, the DC = 0.25 cases, with a quarter of the coolant flow rate, show comparable cooling effec-

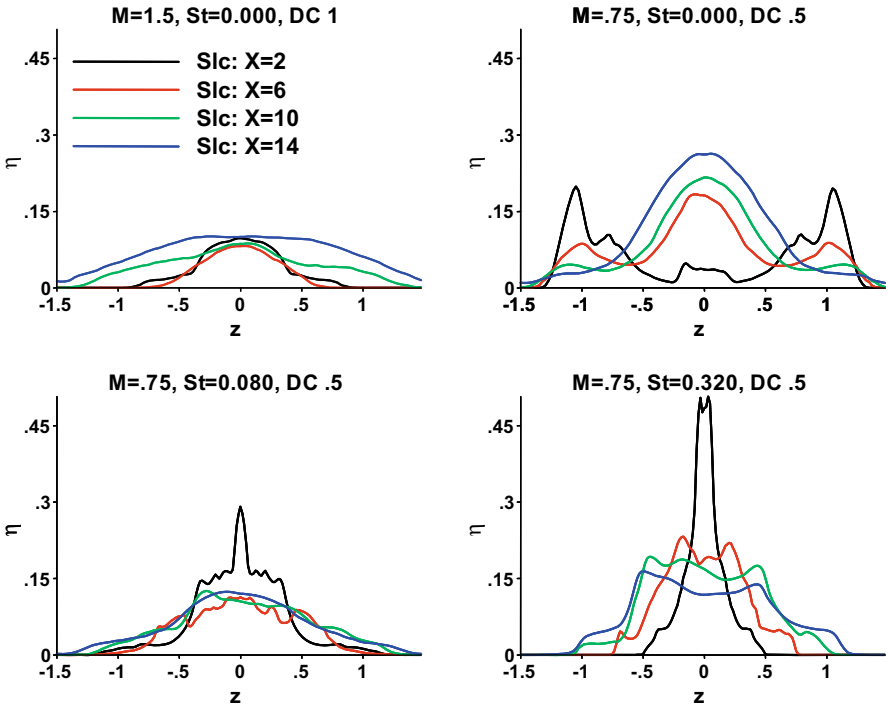

Fig. 9. Spanwise distributions of film-cooling effectiveness.

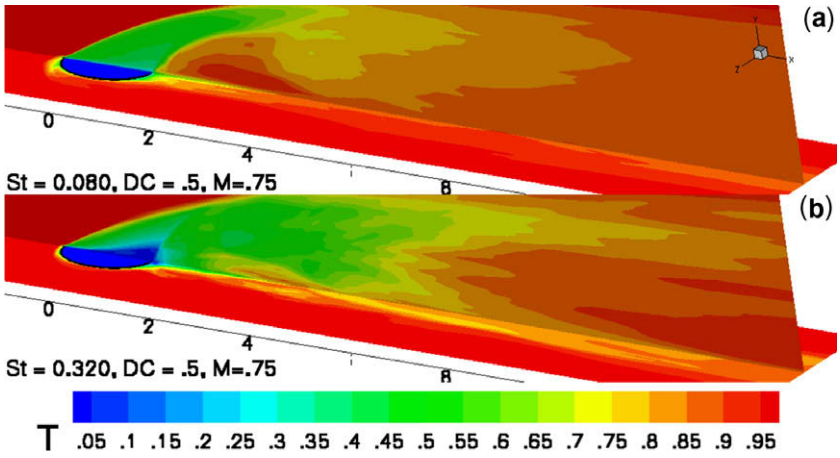

Fig. 10. Contours of time-averaged temperature, DC = 0.5, $M = 0.75$.

tiveness downstream of the coolant hole. However, the unpulsed $M = 0.375$ case shows higher cooling effectiveness, but as mentioned earlier, these low blowing ratios can be impractical to achieve. Fig. 12 shows that the improvement in film-cooling effectiveness at Strouhal number of 0.32 is due to increased downward spreading of the coolant jet. This eliminates the separation zone behind the coolant jet for the 0.32 forcing frequency case.

In order to better understand the mechanisms that lead to improved cooling effectiveness with pulsing, a sequence of instantaneous images of the temperature contour is presented in Fig. 13 for Strouhal number of 0.32 (DC = 0.5, 0.25). From these images it is evident that enhanced vortex dynamics and induction are the reasons for the greater attachment of the jet to the wall. When the pulse is turned "on", a starting vortex is formed (seen clearly in the first frame at $x = 2$) which is a stronger vortex than that formed in the unpulsed system (Fig. 13a). Due to the lower velocities in the separated wake, the part of the vortex on the trailing side of the jet lags the part of the vortex on the leading side, and the vortex structure gets stretched in the streamwise direction. The reorientation alters the

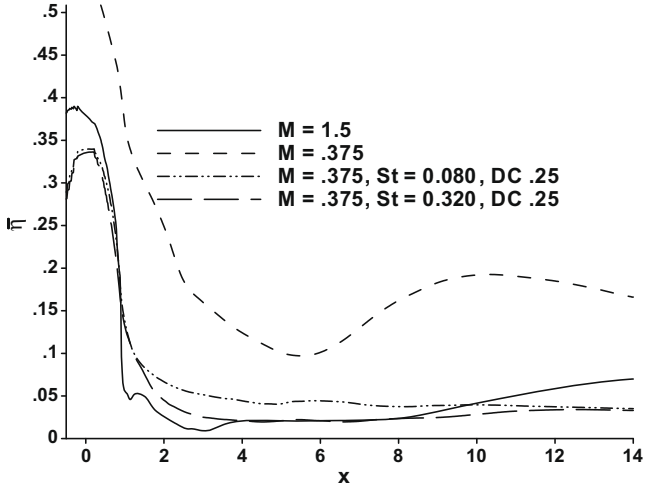

Fig. 11. Spanwise-averaged film-cooling effectiveness, unpulsed and DC = 0.25.

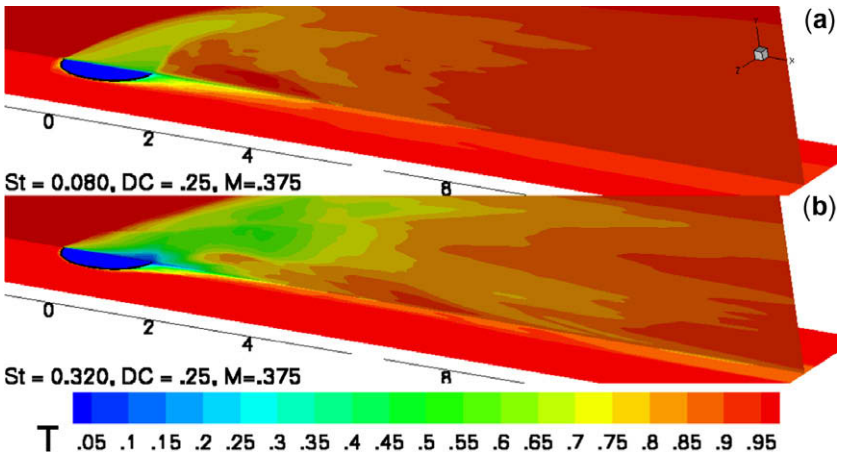

Fig. 12. Contours of time-averaged temperature, DC = 0.25, $M = 0.375$.

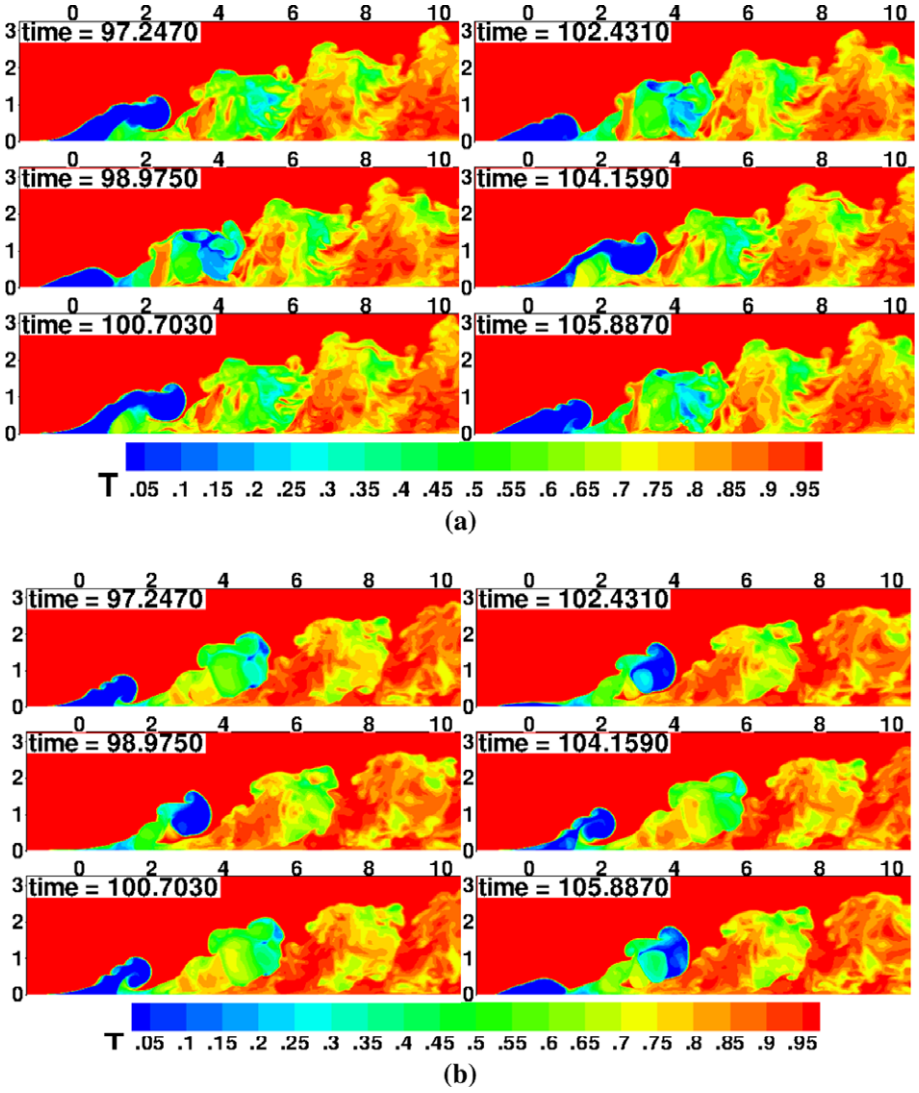

Fig. 13. Temperature contours at different times showing vortex induction towards the wall, (a) St = 0.32, DC = 0.5, horizontal axis is x, vertical axis is y (b) St = 0.32, DC = 0.25, horizontal axis is x, vertical axis is y.

direction of vortex-induction directing it towards the end wall, and causing the coolant jet to reattach. As seen in Fig. 13, the reattached vortex system moves along the end wall providing effective cooling. In the unpulsed case at $M = 1.5$, these mechanisms were missing, and the vortex strength is not strong enough to alter the dynamics of the lifted jet and cause early reattachment. As the Strouhal number is

lowered keeping the duty cycle constant, the duration of the pulses increase. Thus, the frequency of the starting vortex is reduced, and there are longer durations over which no coolant is injected ("off" periods in the pulsing cycle). These two factors lead to the reduced effectiveness that is observed with lower Strouhal numbers.

Fig. 13b shows that the same vortex induction is also present at a duty cycle of 0.25 although it appears to be slightly less effective possibly because the duration of the pulse is reduced by half relative to a duty cycle of 0.5. The coolant packets do not move as close to the end wall as DC = 0.5 case. This indicates the potential of optimizing not only the frequency but also the DC.

8. Conclusion

A study using DNS was performed to investigate the effect of pulsed film-cooling jets on film-cooling effectiveness. Parameters varied during the study were duty cycle and Strouhal number. Improvement in the overall film-cooling effectiveness was found with pulsing relative to the unpulsed flow at the same peak blowing ratio ($M = 1.5$). The range of non-dimensional pulsing frequencies studied varied from 0.004 to 0.32, and best results were obtained at 0.32. When compared with the steady case on the same effective coolant flow rate (or mean blowing ratio) basis, pulsing at a DC of 0.5 showed comparable effectiveness and at a duty cycle of 0.25 showed reduced effectiveness. It should be noted that in many realistic configurations it is not possible to lower the blowing ratio, and pulsing may be the only effective way to enhance film-cooling effectiveness. Further, the recirculation region behind the jet is greatly reduced with pulsing leading to improved film-cooling effectiveness. The present study only examined a small number of pulsed cases and there is a need to optimize the forcing parameters involved.

Acknowledgements

This work was supported by an AFOSR grant from the Rotating and Turbulence Flow Program with Dr. Rhett Smith as the program manager. Discussions with Professor D. Nikitopoulos from LSU and Dr. Richard Rivir from AFRL are gratefully acknowledged.

References

[1] S. Teng, S.D.K. Sohn, J.C. Han, Unsteady wake effect on film temperature and effectiveness distributions for a gas turbine blade, J. Turbomach. 122 (2000) 340–347.
[2] A. Hoda, S. Acharya, Predictions of a film coolant jet in crossflow with different turbulence models, J. Turbomach. 122 (2000) 558–569.
[3] A. Amer, B.A. Jubran, A. Bassam, A.M. Hamdan, Comparison of different two-equation turbulence models for prediction of film cooling from two rows of holes, Numer. Heat Transfer A: Appl. 21 (2) (1992) 143–162.
[4] S. Sarkar, T.K. Bose, Comparison of different turbulence models for prediction of slot-film cooling: flow and temperature field, Numer. Heat Transfer B: Fund. 28 (2) (1995) 217–238.
[5] A. Azzi, M. Abidat, B.A. Jubran, G.S. Theodoridis, Film cooling predictions of simple and compound angle injection from one and two staggered rows, Numer. Heat Transfer A: Appl. 40 (3) (2001) 273–294.
[6] S. Hahn, H. Choi, Unsteady simulation of jets in crossflow, J. Comput. Phys. 134 (1994) 342–356.
[7] F. Muldoon, S. Acharya, Numerical investigation of the dynamical behavior of a row of square jets in crossflow over a surface, ASME Turbo Congress and Expo, 1998, Paper No. 98-GT-019.
[8] M. Tyagi, S. Acharya, Large eddy simulation of rectangular jets in crossflow: effect of hole aspect ratio, in: Proceedings of AFSOR Conference on DNS/LES, Rutgers University, NJ, Kluwer Publisher, June 1999.
[9] M. Tyagi, S. Acharya, Large eddy simulation of a jet in crossflow: freestream turbulence effects, ASME/JSME Fluids Engineering Meeting, San Francisco, July 1999, ASME-FEDSM 99-7799.
[10] M. Tyagi, S. Acharya, Large eddy simulation of a jet in crossflow: large scale turbulence effects, ASME International Mechanical Engineering Congress and Exposition, Nashville, November, 1999.
[11] P. Ajersch, J.M. Zhou, S. Ketler, M. Salcudean, I.S. Gartshore, Multiple jets in a crossflow: detailed measurements and numerical simulation, Paper ASME-95-GT-9, ASME Turbo Congress and Expo 1995, Houston, Texas.
[12] S. Ou, R.B. Rivir, Shaped-hole film cooling with pulsed secondary flow, ASME Turbo Congress and Expo, Barcelona, Spain, May 8–11, 2006.
[13] D. Nikitopoulos, S. Acharya, J. Oertling, F. Muldoon, On active control of film cooling flows, ASME Turbo Congress and Expo, Barcelona, Spain, May 8–11, 2006, Paper ASME-GT2006-90051.
[14] S. Coulthard, R.J. Volino, K.A. Flack, Effect of jet pulsing on film cooling. Part 1: Effectiveness and flowfield temperature results, ASME Turbo Congress and Expo 2006, Barcelona, Spain, May 8–11, 2006.
[15] S. Coulthard, R.J. Volino, K.A. Flack, Effect of jet pulsing on film cooling. Part 2: Heat transfer results, ASME Turbo Congress and Expo 2006, Barcelona, Spain, May 8–11, 2006.
[16] F. Muldoon, Numerical methods for the unsteady incompressible Navier–Stokes equations and their application to the direct numerical simulation of turbulent flows. Ph.D dissertation, Louisiana State University, Baton Rouge, 2004.
[17] F. Muldoon, S. Acharya, Budgets of the k–ε model for film cooling and an improved damping function formulation, AIAA J. 44 (2) (2006) 3010–3031.
[18] S. Acharya, A. Hoda, M. Tyagi, Flow and heat transfer predictions of film cooling, in: R.J. Goldstein, T. Simon (Eds.), Heat Transfer in Gas Turbine Systems, Annals of the New York Academy of Sciences, vol. 934, 2001, pp. 110–125.
[19] T.F. Fric, A. Roshko, Vortical structure in the wake of a transverse jet, J. Fluid Mech. 279 (1994) 1–47.